Document Number**:** H2020-ICT-52/RISE-6G/D2.2

Project Name:
Reconfigurable **I**ntelligent **S**ustainable **E**nvironments for **6G** Wireless Networks (RISE-6G)

Deliverable D2.2

Metrics and KPIs for RISE wireless systems analysis: first results

Date of delivery:	20/07/2021	Version:	7.0
Start date of Project:	01/01/2021	Duration:	36 months

Deliverable D2.2

Metrics and KPIs for RISE wireless systems analysis: first results

Project Number:	101017011
Project Name:	**R**econfigurable **I**ntelligent **S**ustainable **E**nvironments for **6G** Wireless Networks

Document Number:	H2020-ICT-52/RISE-6G/D2.2
Document Title:	Metrics and KPIs for RISE wireless systems analysis: first results
Editor(s):	V. Sciancalepore (NEC)
Authors:	M. Crozzoli (TIM),D. Disco (TIM), T. Svensson (CHAL), A Clemente (CEA), B. Denis (CEA), M.-H. Hamon (ORA), P. Ratajczak (ORA), D.-T. Phan Huy (ORA), G. C. Alexandropoulos (NKUA), K. Katsanos (NKUA), K. Stylianopoulos (NKUA), I. Vinieratou (NKUA), M. Di Renzo (CNRS)
Dissemination Level:	PU
Contractual Date of Delivery:	30/06/2021
Security:	Public
Status:	Final
Version:	7.0
File Name:	RISE-6G_WP2_D2.2.docx

Abstract

According to the objectives of WP2 current document summarizes the first results of the activity devoted to identifying traditional and defining beyond-SoTA relevant performance metrics and target KPIs, to be used by the technical WPs to assess the performance of RISE wireless systems for different scenarios.

A generic DL system model has been described as a basis to provide the definitions for various performance metrics.

The concept of “Area of Influence” as the area of significant improvement of wireless connectivity enabled by the RIS technology has been introduced and some analysis have been performed on it.

Keywords

Beyond-5G; 6G; RIS; KPI; Metrics, Localization, Connectivity

Acronyms

Acronym	Definition
2D	Two dimensional
AO	Alternating Optimization
AoI	Area of influence
B5G	Beyond-5G
BS	Base station
CDF	Cumulative distribution function
CEP	Circular error probability
CPU	Central processing unit
DL	Downlink
E2E	End-to-end delay
EE	Energy efficiency
EE-AoI	Energy efficiency boosted - area of Influence
EMF	Electromagnetic field
EMFE	Electromagnetic field exposure
EMFEE	Electromagnetic field exposure efficiency
EMFEE-AoI	Electromagnetic field exposure efficiency boosted - area of influence
ES	Edge server
HTR	Hit target radius
KPI	Key performance indicator
LB-AoI	Localization boosted - area of influence
LE-AoI	Localization enabled - area of influence
LoS	Line-of-sight
MEC	Multiple-access edge computing
MO	Manifold optimization
MRT	Maximum ratio transmission
MSE	Mean square error
MTBF	Mean-time between failures
NLoS	Non-line-of-sight
NMSE	Normalized mean squared error
PEB	Position error bound
PGA	Projected gradient ascent
PIN	Positive-intrinsic-negative
RIS	Reconfigurable intelligent surface
RISE	RIS-Empowered
RMSE	Root mean squared error
RX	Receiver
SE	Spectral efficiency
SE-AoI	Spectral efficiency-boosted Area of Influence
SINR	Signal-to-noise-plus-interference ratio
SISO	Single input single output
SNR	Signal-to-noise ratio

SoTA	State-of-The-Art
SSE	Secrecy spectral efficiency
UE	User equipment
UL	Uplink

Contents

List of Figures

List of Tables

1 Introduction

The general objective of WP2 is to investigate high relevance Beyond-5G (B5G) scenarios and use cases where RIS technology can be successfully exploited.

Current document summarizes the first results of the activity devoted to identifying traditional and defining beyond-SoTA relevant performance metrics and target KPIs, to be used by the technical WPs to assess the performance of RISE wireless systems for different scenarios.

The document is organized into two main sections: section 2 and section 3.

In section 2 a generic DL system model is defined together with the following metrics and key performance indicators: signal to noise ratio and signal to noise and interference ratio, latency, communication reliability, channel estimation accuracy, localization accuracy and integrity, energy efficiency, electromagnetic field exposure efficiency, secrecy spectral efficiency.

In section 3 the concept of “Area of Influence” as the area of significant improvement of wireless connectivity enabled by the RIS technology is introduced and some analysis are performed on it by starting from the performance analysis of a RIS-Empowered (RISE) system optimized for a nominal intended RX position (the “Spatial Focusing” concept).

2 Metrics and key performance indicators

In this section, we provide first examples of key definitions and key performance indicators (KPI(s)), which are used to evaluate the performance benefits brought by RISs.

In current deliverable, we consider the downlink (DL) direction only. However, for most metrics, the uplink (UL) definition can be derived in a similar manner.

This section is organized as follows: sub-section 2.1 describes the generic DL system model that will be referred to in most consecutive sub-sections; sub-sections 2.2 to 2.11 provide the proposed definitions for various performance metrics.

2.1 Downlink generic system model, signal to noise ratio and signal to noise and interference ratio

We consider a base station (BS) equipped with M antennas, K single-antenna intended user equipment (UE) and an RIS, which is modeled as a planar array with $N = N_x \times N_y$ antenna elements, where N_x and N_y are the number of antenna elements along the x and y axis, respectively.

In this deliverable, we model the BS-to-RIS propagation channel as a Ricean faded channel such that

$$\mathbf{G}_k = \sqrt{\gamma_G}\sqrt{\frac{\kappa_G}{1+\kappa_G}}\,\mathbf{a}(\boldsymbol{\theta}_A)\mathbf{b}(\boldsymbol{\theta}_D)^{\mathrm{H}} + \sqrt{\frac{1}{1+\kappa_G}}\mathbf{H}^{NLoS} \in \mathbb{C}^{N\times M},$$

where γ_G is the average pathloss gain, κ_G is the Rician factor (for $\kappa_G = 0$, the Rayleigh fading case appears, whereas a pure line-of-sight channel happens when κ_G takes large positive values), $[.]^{\mathrm{H}}$ is the Hermitian operation and $\mathbf{H}^{NLoS} \in \mathbb{C}^{N\times M}$ represents the random non-line-of-sight (NLoS) part comprising zero-mean and unit-variance elements. In the latter expression, the antenna array responses at the BS and at the RIS, respectively, for the steering angles θ_A (angle-of-arrival) and θ_D (angle-of-departure), respectively, are defined as:

$$\mathbf{a}(\boldsymbol{\theta}_A) = \left[1, e^{j2\pi\frac{d}{\lambda}\cos(\theta_A)}, \dots, e^{j2\pi\frac{d}{\lambda}(N-1)\cos(\theta_A)}\right]^T \in \mathbb{C}^{N\times 1}$$

and

$$\mathbf{b}(\boldsymbol{\theta}_D) = \left[1, e^{j2\pi\frac{d}{\lambda}\cos(\theta_D)}, \dots, e^{j2\pi\frac{d}{\lambda}(M-1)\cos(\theta_D)}\right]^T \in \mathbb{C}^{M\times 1}$$

with $\frac{d}{\lambda}$ being the ratio between the antenna element spacing and the signal wavelength with $d = \lambda/2$.

The wireless channel between the RIS and each k-th UE is also modeled as Ricean:

$$\mathbf{h}_k = \sqrt{\gamma_k}\sqrt{\frac{\kappa_k}{1+\kappa_k}}\,\mathbf{b}(\boldsymbol{\theta}_k) + \sqrt{\frac{1}{1+\kappa_k}}\mathbf{h}_k^{NLoS} \in \mathbb{C}^{N\times 1},$$

where γ_k is the average pathloss gain, κ_k is the Rician factor, and $\mathbf{h}_k^{NLoS} \sim \mathcal{CN}(0, \boldsymbol{\Sigma})$ represents the random non-line-of-sight (NLoS) part. Finally, we represent the direct link between the BS and UE k as $\mathbf{h}_{d,k} \in \mathbb{C}^{M\times 1}$, which is also modeled as Ricean faded.

Let $\boldsymbol{\Phi} = \mathrm{diag}(\phi_1, \dots, \phi_N) \in \mathbb{C}^{N\times N}$ be the matrix containing the applied phase shifts $\{\phi_n\}_{n=1}^N$ with $|\phi_n|^2 \le 1,\ \forall\, n$ from the RIS. Furthermore, we define the multi-user precoding matrix at the BS as $\mathbf{W} = [\mathbf{w}_1, \dots, \mathbf{w}_K] \in \mathbb{C}^{M\times K}$ with $\|\mathbf{W}\|_F^2 \le P$ (P is the total BS transmit power) and the data symbol vector $\boldsymbol{s} = [s_1, \dots, s_K]^T \in \mathbb{C}^{K\times 1}$ where each s_k is intended for UE k with $\mathbb{E}[|s_k|^2] = 1,\ \forall\, k$.

Lastly, we let n_k denote the additive white Gaussian noise coefficient distributed as $\mathcal{CN}(0, \sigma^2)$. The receive signal at a given UE k is expressed as

$$\boldsymbol{y_k} = \left(\mathbf{h}_k^H \boldsymbol{\Phi} \mathbf{G} + \mathbf{h}_{d,k}^{\mathrm{H}}\right)\mathbf{W}\mathbf{s} + \boldsymbol{n_k} \in \mathbb{C}.$$

Hence, the Signal to Noise Ratio (SNR) of UE k is defined as

$$\mathbf{SNR}_k = \frac{\left|\left(\mathbf{h}_k^{\mathrm{H}} \boldsymbol{\Phi} \mathbf{G} + \mathbf{h}_{d,k}^{\mathrm{H}}\right)\mathbf{w}_k\right|^2}{\boldsymbol{\sigma^2}},$$

and, consecutively, the Signal to Interference plus Noise Ratio (SINR) of UE k is given by

$$\mathbf{SINR}_k = \frac{\left|\left(\mathbf{h}_k^H \boldsymbol{\Phi} \mathbf{G} + \mathbf{h}_{d,k}^{\mathrm{H}}\right)\mathbf{w}_k\right|^2}{\sum_{j \neq k}\left|\left(\mathbf{h}_k^H \boldsymbol{\Phi} \mathbf{G} + \mathbf{h}_{d,k}^{\mathrm{H}}\right)\mathbf{w}_j\right|^2 + \boldsymbol{\sigma^2}} \quad (1)$$

In the next steps of the research activity this definition will be extended to any type of propagation channel.

2.2 Spectral efficiency and throughput

In this sub-section, we provide an example of definition of the **spectral efficiency (SE)** metric, which concerns the rate of reliably-transmitted information over the allocated communication bandwidth B. Formally, the achievable SE with respect to a UE depends on the UE's SINR. For instance, with the notation defined in (1), the achievable SE with respect to a UE *k* is given by

$$\mathbf{SE}_k = \mathbf{log_2}(\mathbf{1} + \mathbf{SINR}_k) \quad (\mathbf{bits/s/Hz}), \quad (2)$$

and accordingly, the *sum-rate over the allocated bandwidth* – i.e., the sum of individual rates for all UE(s), is defined as

$$\boldsymbol{\mathcal{R}} = \sum_k \mathbf{SE}_k .$$

The throughput of the considered system is finally given by:

$$\boldsymbol{T} = \boldsymbol{B\mathcal{R}}.$$

2.3 Latency

Latency is a key performance metric in 5G (and beyond) MEC systems. Several applications (e.g., autonomous driving, industry 4.0, etc.) pose a very strict requirement on the end-to-end (E2E) latency, which in many cases must be in the order of 1ms or even less. The definition of E2E latency in the MEC context depends on the kind of computation offloading request, which can be categorized as either static or dynamic.

2.3.1 Static computation offloading

Static computation offloading deals with short time applications, in which mobile users send a single computation request, typically also specifying a service time. Let $A_k(t)$ be the number of input bits required by the application run by user k at time t, and let $w_k(t)$ be the number of Central Processing Unit (CPU) cycles associated with the computing task. Then, the overall E2E delay of UE k is composed of three terms: (i) an UL communication time $\Delta_k^u(t)$, needed by the device to send the input bits to the BS; (ii) a computation time $\Delta_k^c(t)$, needed by the edge server (ES) to process the input bits and run the specific application; (iii) a DL communication time $\Delta_k^d(t)$, needed by the BS to send the result of computation back to the UE(s).

In summary, the overall E2E latency at time t is given by:

$$\Delta_k(t) = \Delta_k^u(t) + \Delta_k^c(t) + \Delta_k^d(t) = \frac{A_k(t)}{R_k(t)} + \frac{w_k(t)}{f_k(t)} + \frac{B_k(t)}{R_k^d(t)}, \quad (3)$$

where $R_k(t)$ is the uplink rate from UE k to the BS, $f_k(t)$ is the CPU frequency allocated by the edge server to UE k, $R_k^d(t)$ is the downlink rate from the BS to UE k, and $B_k(t)$ is the number of output bits of the application run by the ES on behalf of UE k. In static computation offloading, communication and computation resources are orchestrated to guarantee that the overall E2E delay $\Delta_k(t)$ is less than or equal to an application-dependent requirement, say L_k for all t.

2.3.2 Dynamic computation offloading

In *Dynamic computation offloading*, each device continuously generates data $A_k(t)$ to be processed, sometimes with an unknown rate (e.g., the transmission of a video recorded by a mobile device to be processed by the ES for pattern recognition or anomaly detection). Then, a queueing system is used to model and control the dynamic data generation, transmission, and processing. At each time slot t, each user buffers data in a local queue $Q_k^l(t)$ and transmits them to the AP at the transmission rate $R_k(t)$. The local queue update follows the rule:

$$\boldsymbol{Q_k^l(t+1) = max\left(0, Q_k^l(t) - \tau R_k(t)\right) + A_k(t)}$$

where τ is the duration of the time-slot used for scheduling the resources.

Then, the BS receives data from each device k and send the data to the ES, which processes J_k bits-for-cycle, where J_k is a parameter that depends on the application offloaded by device k. Thus, the computation queue at the ES evolves as:

$$\boldsymbol{Q_k^c(t+1) = \max(0, Q_k^c(t) - \tau f_k(t) J_k) + \min(Q_k^l(t), \tau R_k(t))}$$

Finally, the BS sends back to each user the bits resulting from the computation, draining a downlink communication queue that evolves as:

$$\boldsymbol{Q_k^d(t+1) = \max\left(0, Q_k^d(t) - \tau R_k^d(t)\right) + c_k \min(Q_k^c(t), \tau f_k(t) J_k),}$$

where c_k denotes the ratio between output and input bits of the application required by user k. Thus, the E2E delay experienced by offloaded data is related to the sum of the three queues:

$$\boldsymbol{Q_k^{tot}(t) = Q_k^l(t) + Q_k^c(t) + Q_k^d(t).}$$

In fact, from the Little's law, given a data arrival rate $\bar{A}_k = \mathbb{E}[A_k(t)]$, (where $\mathbb{E}[.]$ is the expectation) the overall long-term average latency experienced by a new data unit from its generation to its computation at the ES is:

$$\boldsymbol{\bar{D}_k = \lim_{T\to\infty} \frac{1}{T} \sum_{t=1}^{T} \mathbb{E}\left[\frac{Q_k^{tot}(t)}{\bar{A}_k}\right]}$$

where the expectation is taken with respect to the radio channel and data arrival statistics.

Thus, in this dynamic context, an average E2E delay constraint can be written as:

$$\boldsymbol{\lim_{T\to\infty} \frac{1}{T} \sum_{t=1}^{T} \mathbb{E}[Q_k^{tot}(t)] \le Q_k^{avg} = D_k^{avg} \bar{A}_k}\ . \quad (4)$$

More sophisticated probabilistic constraints can also be imposed on the maximum tolerable delay.

2.3.3 Expected impact of RIS

Of course, the presence of RISs will impact both UL and DL communication delays, enabling mobile edge computing with low latency guarantees also in the presence of poor wireless channel conditions due to, e.g., blocking events, mobility of the UE(s) and the environment, etc.

2.4 Communication reliability

Given the definitions provided in section 2.1, we define the notion of ***reliability*** of the communication by considering a given minimum SINR threshold denoted as t, which is necessary to decode the incoming signal. We define the set of UE(s) whose received SINR is greater than t as

$$\mathcal{U} = \{k : \mathbf{SINR}_k \geq t\}. \quad (5)$$

RIS-Enabled systems are expected to enlarge the network area in which the received SINR of a given UE in said area is above threshold and thus sufficient for successful decoding of the incoming signal.

2.5 Channel estimation accuracy

For the specific problem of channel estimation, we consider the ***normalized mean squared error*** (NMSE) metric to assess the performance of the estimation process. Specifically, NMSE (in dB) can be defined as

$$\mathbf{NMSE} = \mathbb{E}\left[\frac{10\log_{10}\|\mathbf{H}-\hat{\mathbf{H}}\|_F^2}{\|\mathbf{H}\|_F^2}\right], \quad (6)$$

where $\mathbf{H}$ and $\hat{\mathbf{H}}$ denote the true and estimated channel matrices, respectively, and $\|\cdot\|_F$ denotes the Frobenius norm.

2.6 Localization accuracy

The ***localization accuracy*** is fundamentally determined by the statistics of the localization $\mathbf{e} = \mathbf{x} - \hat{\mathbf{x}}$, comprising horizontal (XY) and vertical (Z) errors.

The statistics include:

- Mean Square Error (MSE): $\mathbb{E}[\mathbf{e}^T\mathbf{e}]$;
- Root MSE (RMSE): $\sqrt{\mathbb{E}[\mathbf{e}^T\mathbf{e}]}$;
- Accuracy (with confidence level α): $e: p(\|\mathbf{e}\| < e) = \alpha$;
- Horizontal accuracy (with confidence level α): $e: p(\|\mathbf{e}_{1:2}\| < e) = \alpha$;
- Vertical accuracy (with confidence level α): $e: p(|e_3| < e) = \alpha$.

The accuracy levels rely on the (empirical) *Cumulative Distribution Function* (CDF) of localization estimation errors. The CDF is often used to characterize characteristic error values (e.g., so-called “worst case” localization errors at arbitrary high CDF values, typically 90% or 99%). Accordingly, they can reflect more accurately effects such as heavy-tailed/asymmetric localization error distributions, beyond indicators such as MSE.

From these fundamental metrics, additional metric such as *Circular Error Probability* (CEP) and *Hit Target Radius* (HTR) can be derived. CEP is defined as the probability for a location estimate to fall into a circle (resp. sphere) of radius R centred around the ground-truth location in 2D (resp. 3D). HTR corresponds to CEP equal to 50%.

The **Position Error Bound** (PEB) indicator is a theoretical performance indicator accounting for the best localization accuracy achievable by any unbiased estimator, assuming the statistics

of available observed/measured radio metrics and, possibly, some a-priori knowledge on user location. The PEB is defined form the Fisher information matrix **J**, which is a theoretical lower bound on the error covariance, under certain technical condition:

$$\mathbf{J}^{-1}(\mathbf{x}) \preccurlyeq \mathbb{E}[(\mathbf{x}-\hat{\mathbf{x}})(\mathbf{x}-\hat{\mathbf{x}})^{\mathbf{T}}].$$

The PEB (expressed in meters) at a location ***x*** is then defined as

$$\mathbf{PEB}(\mathbf{x}) = \sqrt{\mathbf{trace}\left(\mathbf{J}^{-1}(\mathbf{x})\right)} \leq \sqrt{\mathbb{E}[\|\mathbf{x}-\hat{\mathbf{x}}\|^2]}. \quad (7)$$

The PEB can be evaluated as a function of the user location and represented as a heatmap over a scene.

2.7 Localization-related delays

As localization is often time-sensitive and sometimes safety-critical, there are also delay metrics. These include:

- ***First time to fix***: time until the system provides the first location estimate;
- Localization ***latency***: time between a positioning request and the position being available;
- ***Update rate***: time between successive position estimates.

2.8 Localization integrity

In certain critical applications, the localization error cannot exceed certain safe thresholds and the localization service must be available without interruption. Relevant metrics in this regard are:

- ***Reliability***: measured by mean-time between failures (MTBF) or duration of the time the service is available;
- ***Availability***: fraction of the time the service is available.

High reliability means high availability, but not the other way around. Hence, a system that is down (i) every other minute for 1 minute or (ii) every other hour for 1 hour has the same availability, but very different reliability.

2.9 Energy efficiency

In this sub-section, we define the ***Energy efficiency*** (EE) metric for a downlink data communication from a BS to a UE as follows:

$$\boldsymbol{EE = R/P}, \quad (8)$$

where R is the sum data *spectral efficiency* (accounting for *overhead* as in [ZDR+21-1][ZDR+21-2]) in b/s/Hz and P is the total power consumption in watts for providing the target service, as in [HZA+19].

To allow a fair comparison between state-of-the-art systems and beyond state-of-the-art systems, P must include all significant sources of power consumption. In Table 2-1 au-dessous, we provide a first list of contributions to the total power consumption.

	energy spent by	for what	nature of spent energy
$\boldsymbol{P_1}$	BS(s)	Sending DL pilots to UE	Radiated power
$\boldsymbol{P_2}$	UE(s)	Sending UL feedback to base station	
$\boldsymbol{P_3}$	BS (s)	Sending data	
$\boldsymbol{P_4}$	BS (s)	All except radiated power	Hardware

P_5	UE(s)	All except radiated power	
P_6	RIS(s)	Reconfiguring and remaining in a given configuration	Hardware
P_7	BS (s)	Sending RIS command to RIS	Radiated power

Table 2-1 – Sources of power consumption.

With such definition, the power consumptions P^{REF} and P^{RIS} in a network without and with RIS, respectively, are given by the following formulas:

$$P^{REF} = P_1 + P_2 + P_3 + P_4 + P_5$$

and

$$P^{RIS} = P_1 + P_2 + P_3 + P_4 + P_5 + P_6 + P_7$$

Note that the exact expressions of the power consumptions due to radiated power (P_1 to P_3, and P_7), highly differ from one system to another and strongly depend on signalling protocols and overhead. Some detailed examples are available in [ZDR+21-1], [ZDR+21-2] and [HZA+19].

Note that the power consumption due to the RIS hardware (P_6) is expected to increase linearly with the number of unit cells in the RIS.

For instance, in a first example of RIS implementation [FPH+21], where each unit cell of the RIS is reflecting incident waves with a phase-shift that is continuously controlled by four varactors (see Figure 2-1 a), the energy consumption of the RIS can be approximated by [RBF+10][RBF+13]:

$$P_6 \sim P_{cc} + P_{cell} \times N$$

where N is the number of unit cells, P_{cc} is the consumption of the RIS control circuit (mainly a micro-controller connected to all unit-cells), P_{cell} is the consumption per unit-cell (accounting for the varactors, digital potentiometers, logical switches, etc.). Note that such model is used in [HZA+19].

In a second example of RIS implementation based on positive-intrinsic-negative (PIN) diodes, where a unit cell is controlled via two diodes (see Figure 2-1 b), and where the diodes are themselves controlled by using a bias current in the range of 1-20 mA and a forward voltage between 1.33V and 1.45V [CDS+12][CDS+13][DPC+17][DCS+20][CDP+20], the same kind of linear dependency of the power with the number of unit cells N applies. In this implementation,

$$P_{cell} \sim Nbl.Vf.Ibias,$$

where, Nbl is the number of bias lines for unit-cells, Vf is the forward voltage and $Ibias$ is the bias current.

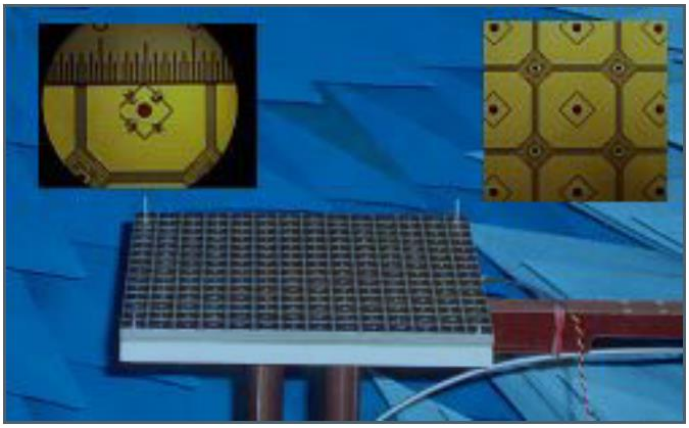

a) Varycap based RIS

b) PIN-Diode based RIS

Figure 2-1 – Example of RIS hardware implementations with a) Varycap [RFB+10] and b) PIN diode [CDS+12].

Also, to this stage, it is not yet clear, whether some P_i's can be neglected compared to others. For instance, it has to be checked during the project whether the hardware consumption of RIS(s) can be neglected or not compared to the hardware consumption of BS(s) and UE(s) (i.e. it has to be verified whether $P_6 \ll P_5$ and $P_6 \ll P_4$ applies).

2.10 Electromagnetic field exposure efficiency

In this sub-section, in addition to the DL case, we also consider the uplink case.

We first consider as a target service, a DL data communication towards an intended user. We also consider a non-intended user who is potentially exposed to the electromagnetic field (EMF) generated by this link. For this target service, we propose the following definition of the ***DL electromagnetic field exposure (EMFEE)*** or **inter EMFEE**:

$$\boldsymbol{DL - EMFEE = R^{DL}/X^{NI}}, \tag{9}$$

where R^{DL} is data rate that is delivered to the intended user and X^{NI} is the EMF to which the non-intended user is exposed. In the case where we are considering multiple non-intended users, X^{NI} is the EMF of the most exposed one.

We then consider as a target service, an UL data communication issued by an intended user. In this case, the intended user is also the exposed one. For this target service, we propose the following definition of the ***UL EMFEE*** or **self EMFEE**:

$$\boldsymbol{UL - EMFEE = R^{UL}/X^{I}}, \tag{10}$$

where R^{UL} is data rate that is transmitted by the intended user and X^{I} is the EMF to which the intended user is exposed.

2.11 Secrecy spectral efficiency

The ***Secrecy spectral efficiency*** (SSE) metric is defined as the difference between the intended receiver (RX)'s rate R_I, referring to the legitimate link, and the non-intended RX's rate R_{NI}, referring to the link between the legitimate transmitter and the eavesdropper. When this difference results in a negative number, it means that no security is guaranteed, and the SSE is defined as zero.

Putting all above together, the mathematical definition of SSE is given by

$$\boldsymbol{SSE = \max(0, R_I - R_{NI})} \quad \textbf{(bits/s/Hz)} \tag{11}$$

where $R_I = \log_2(1 + SNR_I)$ and $R_{NI} = \log_2(1 + SNR_{NI})$ with SNR_l being defined as in sub-section 2.1, while SNR_{NI} is defined in a similar way by considering the BS to the non-intended user direct channel $\mathbf{g}_d$ and the RIS to the non-intended user channel $\mathbf{g}$.

3 RIS Area of Influence

In this section, we investigate the spatial distribution of the RIS-optimized performance over a geographical area under consideration for the connectivity-related metrics and KPIs of subsections 2.1 to 2.11. To that end, we first study how the performance of a RIS-empowered system optimized for a nominal intended RX position is distributed in space (i.e. the "***Spatial Focusing***") in sub-section 3.1 and its subsections. Building on those results, we define the more general notion of the "***Area of Influence***" which concerns the areas of significant improvement of wireless connectivity, when optimizing for the entirety of the area under consideration, instead of a single nominal RX position.

3.1 Investigation of the RIS spatial focusing

This sub-section, thanks to simulations of the following subsections, shows that the improvement brought by the RIS optimization, with respect to each of the considered connectivity metrics, is localized in space. In detail, we devise a common setup comprised of a single TX, a single RIS and a single intended RX, and potentially an attenuator/blocker, and we optimize the system parameters for the position of the nominal intended RX. We visually demonstrate that, for all metrics and considering a Ricean-faded channel with a string LoS component, the substantial improvement of the performance, in general, lies on the path of the RIS-RX link, as well as the TX-RIS link, in the cases without the attenuator.

3.1.1 Spatial focusing of SE

To investigate the spatial locality of the SE improvement, we first consider a scenario where an *M*-antenna BS transmits data to a single-antenna RX, under either the absence or the presence of an RIS comprising of L unit elements. Specifically, the problem of maximizing the achievable rate is formulated first and then solved with optimization variables the BS precoder $\mathbf{w} \in \mathbb{C}^{M\times 1}$ and the passive beamforming diagonal matrix $\mathbf{\Phi} \in \mathbb{C}^{L\times L}$ for the surface. We denote $\mathbf{h}_d \in \mathbb{C}^{1\times M}$, $\mathbf{h} \in \mathbb{C}^{1\times L}$ and $\mathbf{H}_1 \in \mathbb{C}^{L\times M}$, as the matrices of the direct BS-to- RX, RIS-to-RX and the BS to RIS propagation channel, respectively.To this end, the joint design of these variables is expressed as

$$\boldsymbol{max}_{\mathbf{w},\mathbf{\Phi}} \ \boldsymbol{log}_2\left(\mathbf{1}+\frac{\boldsymbol{P}}{\boldsymbol{\sigma^2}}|(\mathbf{h}_d+\mathbf{h}\mathbf{\Phi}\mathbf{H_1})\mathbf{w}|^2\right)$$
$$\boldsymbol{s.t.}: \|\mathbf{w}\|^2 \leq \mathbf{1}, \ \left|\mathbf{\Phi}_{l,l}\right| = \mathbf{1} \ \forall \ \boldsymbol{l} = \mathbf{1}, \mathbf{2}, \ldots, \boldsymbol{L}.$$

In the case where the RIS is not present, the above problem reduces to a special version which is solved by setting the precoder $\mathbf{w}$, equal to the Maximal Ratio Transmission (MRT) precoding vector considering the direct channel $\mathbf{h}_d$. Next, to solve the above joint problem, an Alternating Optimization (AO) approach is adopted, according to which each variable is solved separately until a convergence criterion is met. Then, $\mathbf{w}$ can be solved in closed form, by considering MRT precoding (based on the channel: $\mathbf{h}_d + \mathbf{h}\mathbf{\Phi}\mathbf{H_1}$), and for $\mathbf{\Phi}$ a Riemannian Manifold Optimization (MO) approach is utilized.

To illustrate the results for both above scenarios, we consider a square grid area with each side being equal to 25m, where the BS is fixed at the point [0 m, 10 m] of the *xy*-plane. Also, the optimization problem is solved for a certain position of RX, whose coordinates are [15 m, 5 m]. Then, the obtained active and passive beamforming vectors of the nominal position are used to compute the achievable rates for all possible locations inside the grid, to reveal the locality in the considered two-dimensional (2D) area and observe the influence of an RIS when present and located at [10 m, 0 m] The other simulation-setup parameters are presented in the table below and the results are averaged over 100 channel realizations.

Parameter	Value	Parameter	Value
$\boldsymbol{P}$	30 dBm	M	8

σ^2	-90 dBm	L	100
κ	13.2 dB	Pathloss Exponent	2.4

Table 3-1 – Simulation parameters.

Next, in Figure 3-1 below the 2D heatmap for the achievable SE in bits/s/Hz and its spatial distribution is illustrated for the cases of the absence and presence of an RIS. Since the LoS component is strong, due to the considered Rician factor κ, some beam patterns appear in the grid area, which are stronger in terms of rate values at the direction that connects the BS with RX's nominal position. On the other hand, when placing an RIS at the location [10, 0], it is depicted in the right subfigure, that almost the whole area gets boosted, in the sense that larger EE values are observed when compared to the case without RIS. Moreover, an enhanced line pattern of rate values is observed as well, at the line that connects the RIS with RX's nominal position. Moreover, it is observed that in contrast to the case of the absence of an RIS, the main beam pattern starting from the BS and heading to nominal RX, is shifted on the right subfigure heading to the RIS which is in turn concentrated to nominal RX's position. This is reasonable, since it shows that the optimization process is in terms of the compound channel $\mathbf{h}_d + \mathbf{h}\boldsymbol{\Phi}\mathbf{H}_1$.

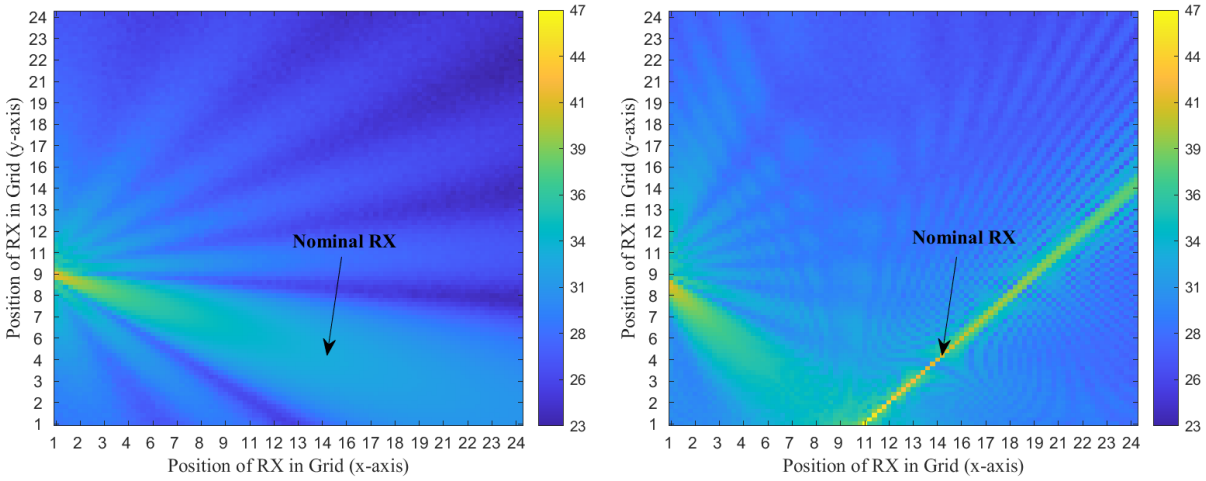

Figure 3-1 – SE values on a 2D grid.
(Left) without the presence of a RIS. (Right) with a RIS placed at [10, 0].

To further show the effects of spatial focusing for SE when an RIS is present, we next introduce an attenuation factor for the LoS component of the direct channel $\mathbf{h}_d$ between the BS and RX, which is considered equal to 0.01 (i.e., 100 dB attenuation). The results for this case are presented in Figure 3-2, where it is evident that in the case of attenuation there is nearly no LoS channel component and the channel's Rayleigh component is thus dominant, such that small SE values are observed. However, when placing an RIS the whole area gets boosted and especially the line that connects the surface with the nominal RX's position.

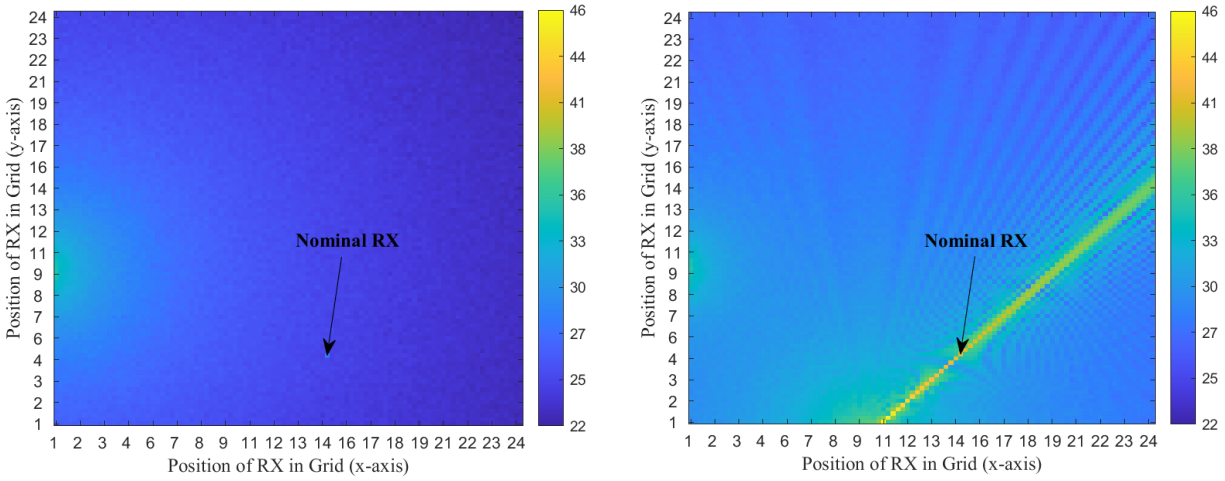

Figure 3-2 – SE values on a 2D grid.
(Left) without the presence of a RIS. (Right) with a RIS placed at [10, 0] with attenuation.

3.1.2 Spatial focusing of SSE

To investigate the spatial locality of the SSE improvement, a scenario with an *M*-antenna BS is considered which attempts to transmit secret single stream data to a single-antenna RX, where a single-antenna eavesdropper is present at the system. To further safeguard the legitimate system [AKW+21], an RIS is also employed under the control of the BS that designs both the precoding vector $\mathbf{w}$ and the passive beamforming diagonal matrix $\mathbf{\Phi}$. Specifically, using the same notations $\mathbf{g}_d$ and $\mathbf{g}$, as in sub-section 2.11, for the BS to the non-intended user direct channel and the RIS to the non-intended user channel, respectively. these design variables are modelled as the solution to the following optimization problem

$$\boldsymbol{max}_{\mathbf{w},\mathbf{\Phi}} \ \boldsymbol{log}_2\left(\mathbf{1}+\frac{\boldsymbol{P}}{\boldsymbol{\sigma}^2}|(\mathbf{h}_d+\mathbf{h}\mathbf{\Phi}\mathbf{H}_1)\mathbf{w}|^2\right)-\boldsymbol{log}_2\left(\mathbf{1}+\frac{\boldsymbol{P}}{\boldsymbol{\sigma}^2}|(\mathbf{g}_d+\mathbf{g}\mathbf{\Phi}\mathbf{H}_1)\mathbf{w}|^2\right)$$
$$\boldsymbol{s.t.}: \|\mathbf{w}\|^2 \leq \mathbf{1}, \ \left|\mathbf{\Phi}_{l,l}\right| = \mathbf{1} \ \forall \ \boldsymbol{l} = \mathbf{1},\mathbf{2},\ldots,\boldsymbol{L},$$

where the first term in the objective expresses the legitimate rate and the second one the eavesdropper's rate; their subtraction is the instantaneous SSE performance metric as defined in sub-section 2.11. The solution approach to the above problem is AO, due to the coupled variables and the non-convex objective/constraints. Specifically, to find $\mathbf{w}$ for a fixed $\mathbf{\Phi}$ it suffices to observe that it can be given as the unit-norm eigenvector of the matrix

$$\left(\mathbf{I}_N+\frac{\boldsymbol{P}}{\boldsymbol{\sigma}^2}\tilde{\mathbf{g}}^H\tilde{\mathbf{g}}\right)^{-1}\left(\mathbf{I}_N+\frac{\boldsymbol{P}}{\boldsymbol{\sigma}^2}\tilde{\mathbf{h}}^H\tilde{\mathbf{h}}\right),$$

which corresponds to its largest eigenvector, and $\tilde{\mathbf{g}} = \mathbf{g}_d + \mathbf{g}\mathbf{\Phi}\mathbf{H}_1, \tilde{\mathbf{h}} = \mathbf{h}_d + \mathbf{h}\mathbf{\Phi}\mathbf{H}_1$. Next, for a fixed $\mathbf{w}$, $\mathbf{\Phi}$ can be found based on a Riemannian MO or Projected Gradient Ascent (PGA) approach.

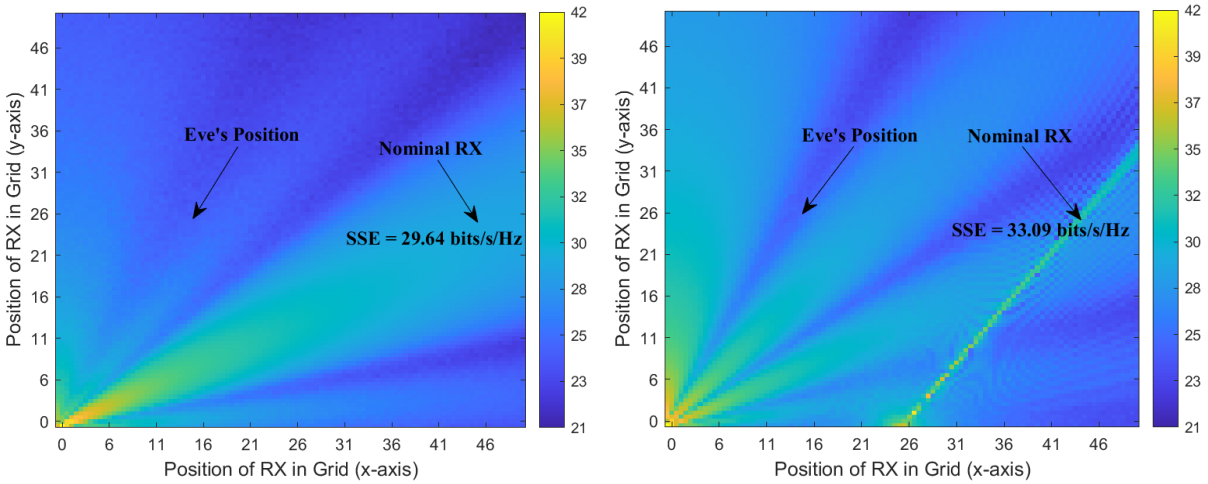

Figure 3-3 – SSE values on a 2D grid with in the presence of an eavesdropper (Eve). (Left) without the presence of a RIS. (Right) with a RIS placed at [0, 25].

In Figure 3-3, the results for the SSE are depicted in the case of the absence (on the left) and the presence (on the right) of an RIS with 100 unit elements. The simulation parameters are set similar to those given in Table 3-1. The eavesdropper's position is at the point [10.5 m, 20.5 m] from the BS which is placed at the origin. Also, the nominal position of RX is at [40.5 m, 20.5 m]. When a non-intended user is present even closer to the BS than RX, it is observed that the presence of an RIS boosts the whole area with higher SSE values. Interestingly, a strong beam pattern is observed in the direction which connects the RIS with RX.

3.1.2.1 Spatial focusing of communication reliability

Given the definitions provided in sub-section 3.1.1 and sub-section 2.1, the receive signal at a given position k is given by:

$$y_k = \left(\mathrm{h}_{d,k} + \mathrm{h}_k \Phi \mathrm{H}_1\right)\mathrm{w}s + n \in \mathbb{C}$$

where s is the transmitted symbol with $\mathbb{E}[|s|^2] = 1$ and n is an additive white Gaussian noise term with variance σ^2.

Hence, the SNR in position k is given by

$$\mathbf{SNR}_k = \frac{\left|\left(\mathbf{h}_{d,k} + \mathbf{h}_k \boldsymbol{\Phi} \mathbf{H}_1\right)\mathbf{w}\right|^2}{\boldsymbol{\sigma}^2}.$$

Assuming the case of a single RX and using the notion of communication reliability in sub-section 2.4, we redefine the set of positions where the signal is received with a given minimum SNR, which is necessary to decode the incoming signal as

$$\boldsymbol{\mathcal{U}} = \{\boldsymbol{k} : \mathbf{SNR}_{\boldsymbol{k}} \geq \boldsymbol{t}\}.$$

The considered simulation scenario is the one described in sub-section 3.1.1 with the channel parameters in Table 3-1. Furthermore, we set $t = 100$ dB. We optimize the RIS phase shifts and BS precoding for the nominal RX position as described in sub-section 3.1.1.

Next, we evaluate the SNR received by a receiver located in any other position identified by the regular lattice for the optimized RIS and BS configuration of the previous subsection.

To investigate the spatial localization of the reliability performance, we use a binary contour plot in 2D, which is provided in the following. In particular, we show the 2D area where the two following conditions are met simultaneously: (i) given SNR threshold is reached thanks to the use of RIS, (ii) a standard system utilizing only precoding at the BS does not attain such minimum acceptable value.

In Figure 3-4, we analyze the case where there is no attenuation between the BS and the nominal RX position. Thanks to the passive beamforming at the RIS, the 2D area in which the received SNR is above the threshold t is enlarged in both the area around the direct link between the BS and the RIS and in the direction of the nominal RX position w.r.t the RIS.

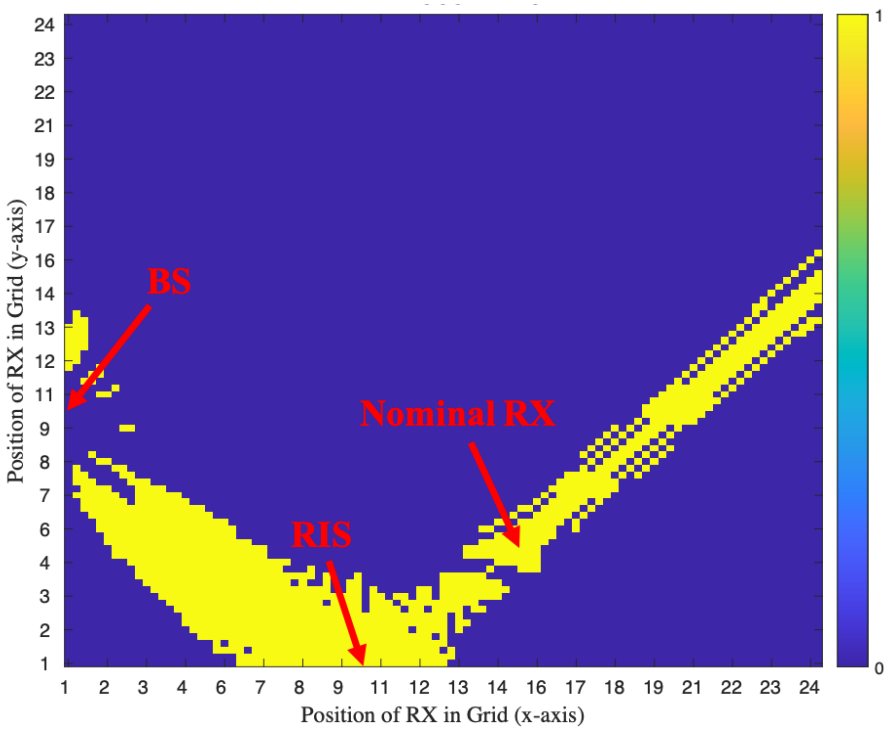

Figure 3-4 – DL case only: example of achievable Reliability values in the absence of attenuators, where thanks to the RIS the received SINR is sufficient for successful decoding of the incoming signal whereas it is not with the standard technology.

Lastly, Figure 3-5 shows the spatial localization of the reliability metric in the case when there is an attenuator in the LoS link between the BS and the nominal RX position. We observe that due to the presence of the attenuator the substantial improvement is limited to the close-proximity to the RIS and along the direction of the nominal RX position w.r.t the RIS, i.e., along the direction of beamforming at the RIS.

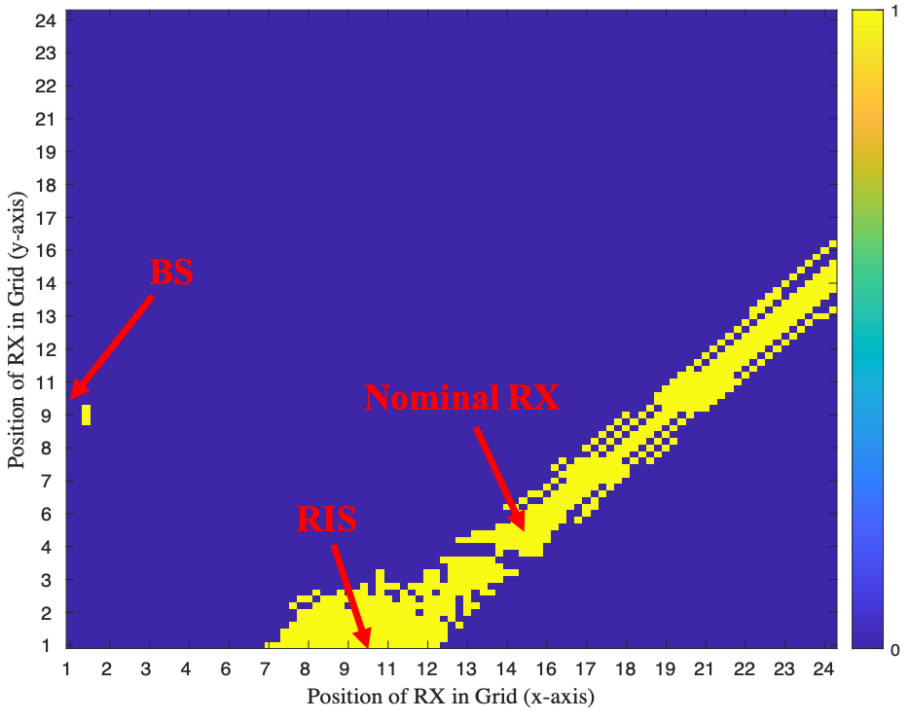

Figure 3-5 – DL case only: example achievable reliability values in the presence of an attenuator, where thanks to the RIS the received SINR is sufficient for successful decoding of the incoming signal whereas it is not with the standard technology.

3.1.2.2 Spatial focusing of latency

In this sub-section, we evaluate the effect of RIS in boosting latency for a nominal RX position. Thus, given the SNR definition given in sub-section 2.1 the communication latency (expressed in seconds) at position k, needed to transmit A_k bits over a channel with bandwidth B, is given by

$$L_k = \frac{A_k}{B\, log_2\left(1 + \frac{\left|\left(\mathbf{h}_{d,k} + \mathbf{h}_k \Phi \mathbf{H}_1\right)\mathbf{w}\right|^2}{\sigma^2}\right)}.$$

Assuming the case of a single RX and using the aforementioned definition of communication latency, we redefine the set of positions where L_k is guaranteed to be below a given threshold:

$$\mathcal{U} = \{k : L_k \leq l\}.$$

The considered simulation scenario is the same used in the previous sub-section, obtained optimizing the RIS phase shifts and BS precoding for the nominal RX position as described in sub-section 3.1.1. Then, we evaluate the latency perceived by a receiver located in any other position identified by the regular lattice for the given RIS and BS configuration. The parameters used for the simulation are $A_k = 1$ Mbit and $B = 30$ MHz. The latency constraint is set to $l = 1$ ms.

To assess the spatial localization of the latency boost given by the RIS, a 2D representation visualizing and quantifying the regions of space where the optimized RIS for the single nominal RX position provides a substantial improvement. In particular, using a 2D binary contour plot, we illustrate the regions where the two following conditions are met simultaneously: (i) the given latency constraint is met thanks to the use of the RIS, (ii) a standard system would fail in obtaining the desired performance.

In Figure 3-6, we illustrate the acceptable latency values in a scenario where there is no attenuation between the BS and the nominal RX position. As we can see from Figure 3-6, the 2D latency boosted area is enlarged in both the area around the direct link between the BS and the RIS and in the direction of the nominal RX position w.r.t the RIS.

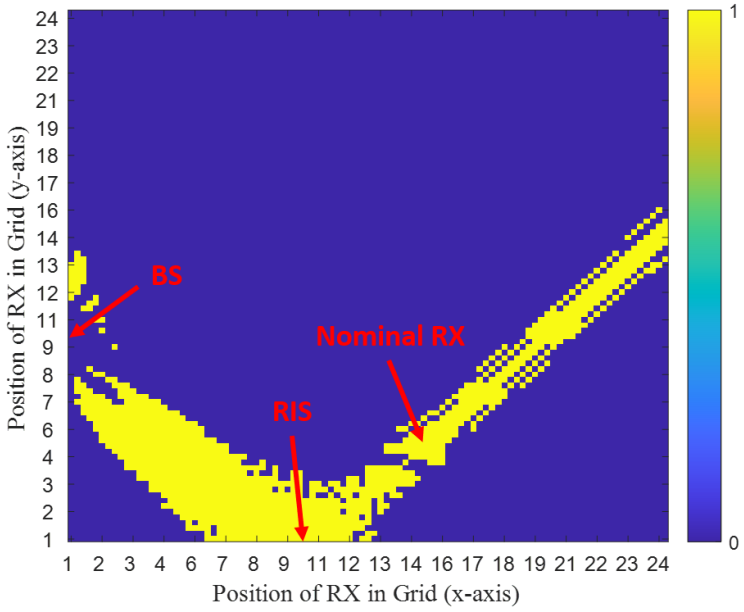

Figure 3-6 – Example of acceptable latency values in the absence of attenuators, where thanks to the RIS the perceived latency meets the desired performance constraint.

Finally, Figure 3-7 shows the acceptable latency values in the case when there is an attenuator in the LoS link between the BS and the nominal RX position. From Figure 3-7, we notice that, similarly to what happens for the reliability case of the previous subsection, the improvement of latency is limited to the close-proximity to the RIS and along the direction of beamforming at the RIS.

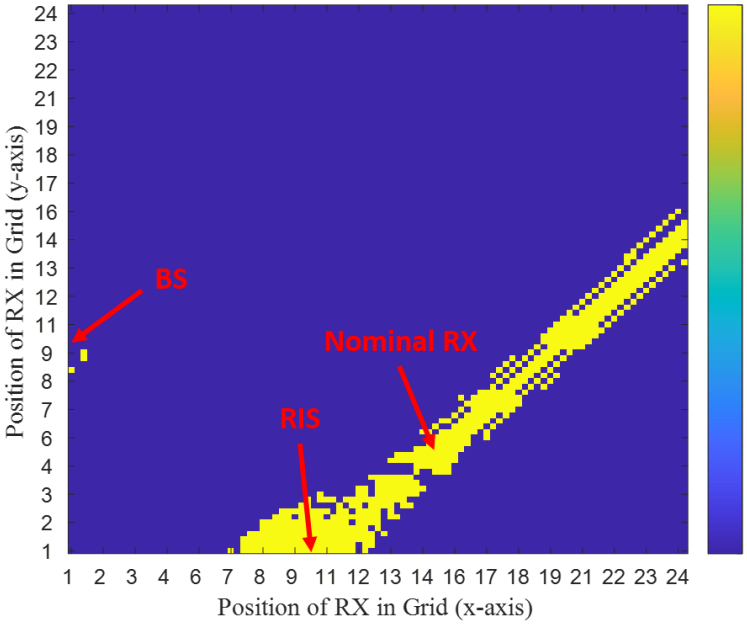

Figure 3-7 – Example of acceptable latency values in the presence of attenuators, where thanks to the RIS the perceived latency meets the desired performance constraint.

3.2 Characterisation of the area of influence

3.2.1 EE-boosted area of influence

We recall that the EE of a DL communication between the network and a target or *intended* user is the ratio of the spectral efficiency delivered to the target user divided by the total power consumed in the radio network for that purpose.

The ***EE boosted area of influence*** (EE-AoI) is a representation visualizing and quantifying in which *locations of the target user*, RIS could improve significantly *the nominal EE of a standard system/technology*. In other terms, out of the EE-AoI, there is no way for the RIS to improve significantly the EE.

It can be typically represented as a binary contour plot in 2D as illustrated in Figure 3-8 below with a RIS consisting of a uniform linear array of 16 unit-cells (10 dBi directional patch antennas) spaced by half a wavelength and with ideal phase-shift control. In the AoI, *the target user* can experience a received power that is *at least boosted by 3 dB* when the RIS is present compared to when the RIS is absent. The computed received power with RIS, is an upper bound, obtained with RIS weights making sure that all the paths (direct source-target user, reflected paths) combine coherently at the target user. Note that in Figure 3-8, the AoI is composed of two separate areas: a tiny one, close to the RIS and in visibility of the source, and a larger one, in the visibility of the RIS and in non-line of sight of source, due to a blocking wall. Hence, *the EE-AoI of a RIS depends on its propagation environments and especially on blockers*.

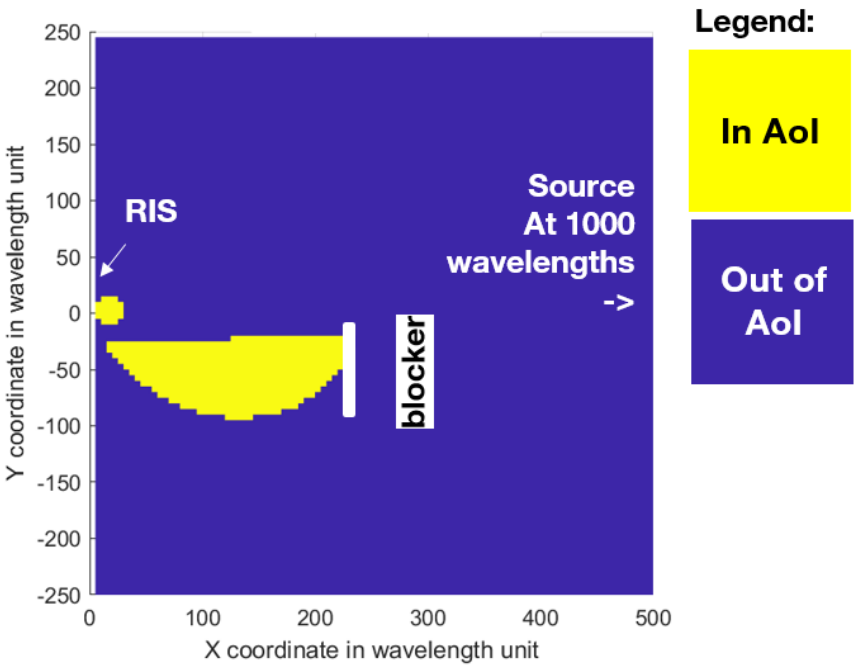

Figure 3-8 – Example of EE-boosted area, where the received power at the target user has been boosted by at least 3 dB.

3.2.2 SE-boosted area of influence

As a further study on the locality of an RIS and how it formulates the space around it, we examine the SE in a sub-grid of the considered grid in Section 3.1.1. Specifically, instead of using the solution given at a nominal position of the RX which results in SE spatial focusing, in this subsection we solve the optimization problem for each position of the sub-grid and then plot the 2D contour figures as shown in Figure 3-9 and Figure 3-10. Figure 3-9 depicts the case when an RIS is not present in the considered system, for the case of a strong LoS component for the

direct channel $\mathbf{h}_d$, as well as the case where the attenuation factor of Section 3.1.1 is considered. As shown, it is evident that when an attenuator is present, the SE for each grid position is smaller than the case without the attenuator.

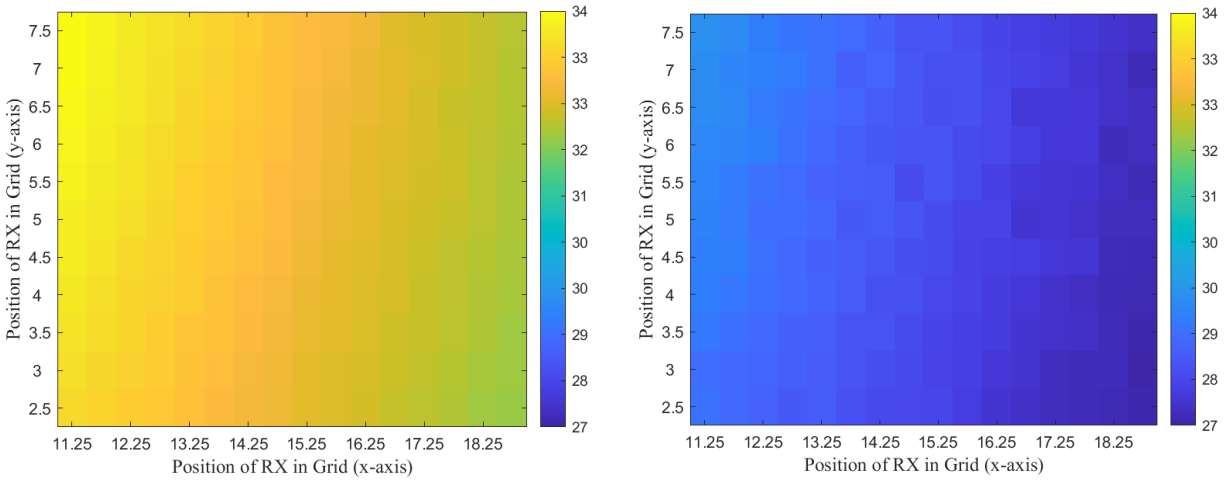

Figure 3-9 – SE on a 2D sub grid without an RIS. (Left) without attenuation factor for the direct link between BS and RX. (Right) with attenuation factor equal to 0.01.

On the other hand, when an RIS is present (Figure 3-10) the whole area is boosted in terms of the higher achievable rates' values that are observed. Moreover, both subfigures are very close to each other since the effect of the RIS is almost the same either in the case without attenuator or with. Finally, it is observed that the higher values in both heatmaps of Figure 2-11, are observed towards the location of the RIS, which is placed outside the depicted sub grid.

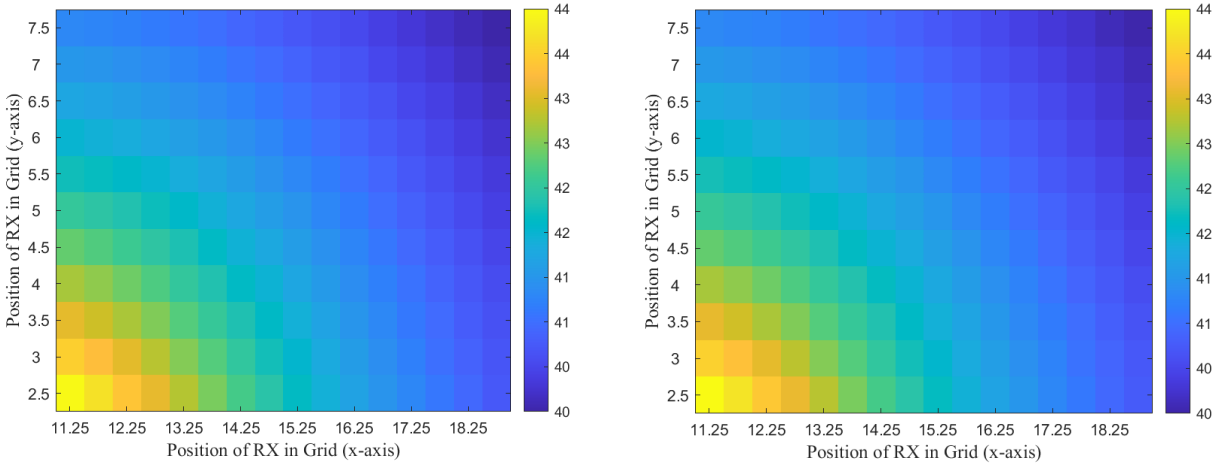

Figure 3-10 – SE on a 2D sub grid with the presence of an RIS. (Left) without attenuation factor for the direct link between BS and RX. (Right) With attenuation factor equal to 0.01.

3.2.3 SSE-boosted area of influence

As another example for the AoI of an RIS and SSE, we next consider a sub grid of the one in Figure 3-3 and solve the corresponding optimization problem for each position of it, to examine the effect of an RIS. As it is shown, when an RIS is not present the SSE values are much smaller than the case where an RIS is present, which shows how an RIS boosts the area under consideration. Moreover, it is also observed that a line pattern is formulated in both cases, but in a different way (since their slopes are different). In the case without an RIS, the formulated line pattern matches with the direction of the line which connects the BS and the intended RX, since

the RX is placed at the centre of the sub grid. Therefore, when the eavesdropper lies along this line, smaller secrecy rate values are observed. Similarly, when an RIS is placed on the wide grid, the line with smaller secrecy rate values lies on the direction that connects the RIS with the RX and accordingly when E is located at those positions.

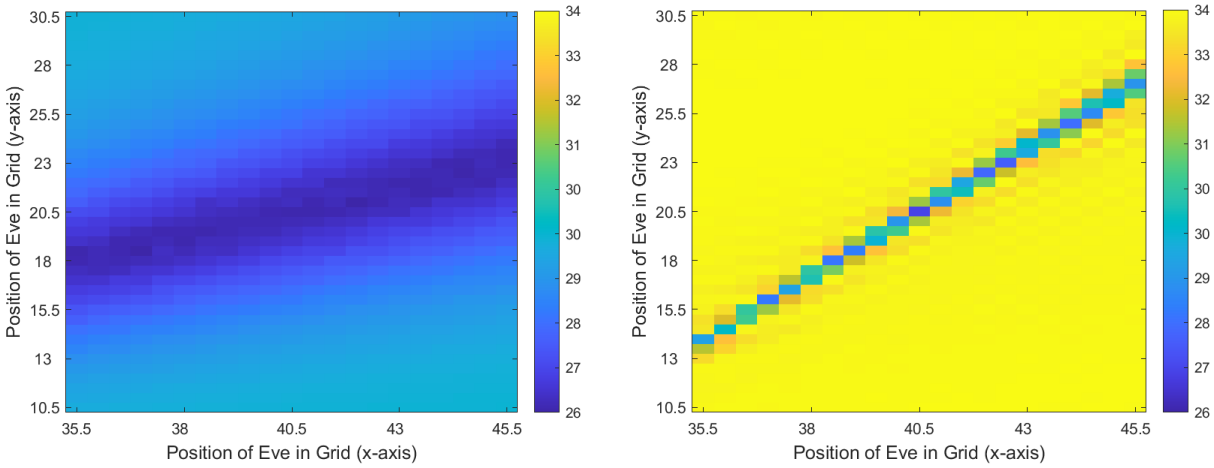

Figure 3-11 **- SSE Secrecy Spectral Efficiency on a 2D sub grid without an RIS (Left). With an RIS (Right).**

3.2.4 EMFEE -boosted area of influence

We recall that the EMFEE of a DL communication between the network and a target user is the ratio of the spectral efficiency delivered to the target user, divided by the EMFE of an exposed non-intended user (see sub-section 2.10).

The **EMFEE-boosted area of influence** (EMFEE-AoI) is a 2D representation visualizing and quantifying in which locations of the exposed non-intended user RIS would reduce the nominal exposure of a standard system/technology. In other terms, out of the EMFE-AoI there is no way for the RIS to reduce significantly the exposure.

It can be typically represented as a binary contour plot in 2D as illustrated in Figure 3-12 below with a RIS consisting of a uniform linear array of 16 unit-cells (10 dBi directional patch antennas) spaced by half a wavelength and . In the AoI, the *non-intended user* can experience a received power that is *at least reduced by 3 dB* when the RIS is present compared to when the RIS is absent. The computed received power with RIS, is an upper bound, obtained with RIS weights making sure that all the reflected paths combine coherently together, at the non-intended user, but *in opposition* to the direct source-to-user path. Figure 3-8, the AoI is, composed of two separate areas: a tiny one, close to the RIS and in visibility of the source, and a larger one, in the visibility of the RIS and in non-line of slight of source, due to a blocking wall. Hence, *the EMFEE-AoI of a RIS depends on its propagation environments, and especially on blockers***.**

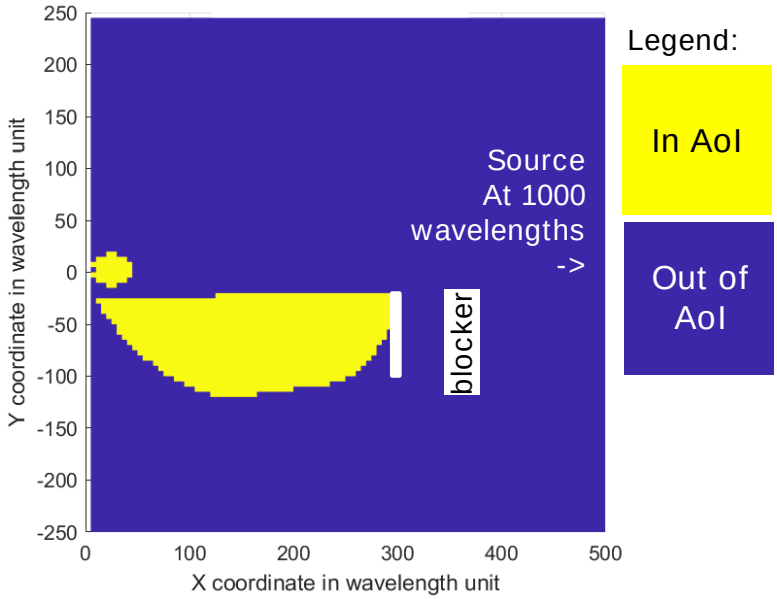

Figure 3-12 – DL case only, Example of EMFEE-AoI where the received power at the exposed non-intended user has been reduced by at least 3 dB

3.2.5 Localization-Enabled Area of Influence

The ***Localization-enabled area of influence*** (LE-AoI) is a 2D representation intended to visualize and quantify where RIS can restore *service coverage & continuity*, when conventional localization is not feasible or strongly degraded, typically if:

- The number of active BS(s) is by default insufficient to ensure non-ambiguous localization;
- The number of BS(s) is sufficient, but the system is facing local blockage situations over one or several radio links.

It can be typically represented as a binary contour plot in 2D, accounting for the area where localization is theoretically feasible (e.g. where PEB is defined) and/or where the achievable error is below a certain a-priori threshold (i.e., where 2D-RMSE or PEB < Target).

Note that the concept of AoI can refer to the aggregated beneficial effects of multiple RISs that are controlled simultaneously in a given environment (not restricting to single-RIS).

A. *Example of PEB with 1 single BS and 1 RIS in reflection mode*

In Figure 3-13 and Figure 3-14, we show two examples of PEB contour map characterizing the localization error over a 2D scene for a RIS-enabled single-BS single input single output (SISO) system, with random and directional RIS phase profiles respectively.

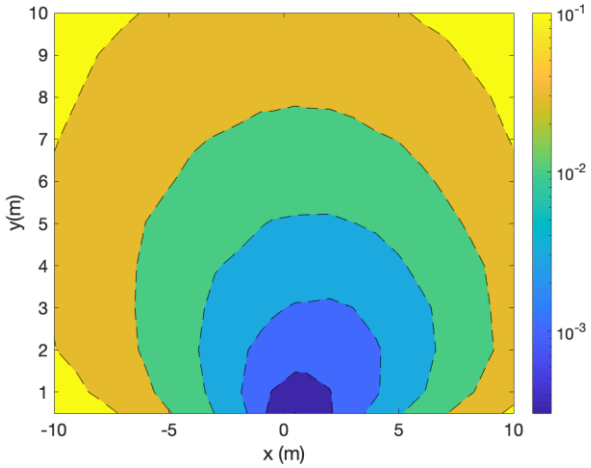

Figure 3-13 – Example of PEB for an RIS-enabled SISO system with random RIS configuration, RIS at the origin, UE on the plane [x, y, -y], and BS at [5, 5, 0].

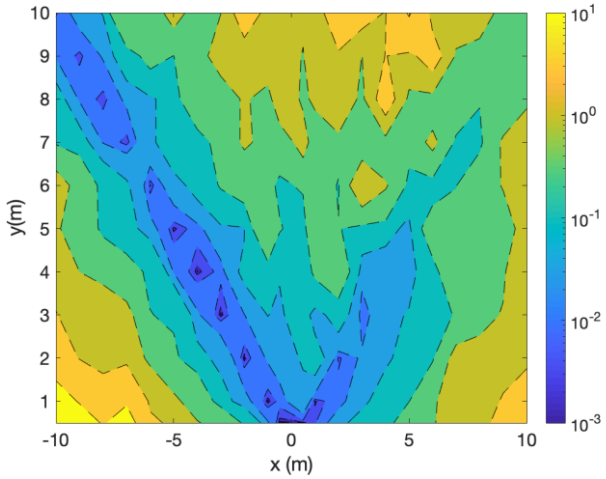

Figure 3-14 – Example of PEB for an RIS-enabled SISO system with directional RIS configuration directed at [-1, 1, -1].

B. Example of PEB with multiple RISs in receive mode

In Figure 3-15 (a)-(c), according to an indoor localization with multiple RISs in reception mode, the PEB in dB is shown for a UE positioned on the z=5m plane. Free space pathloss is considered and LoS channels. 3 RISs are deployed, equipped with single RX RF chains, with 64 elements each, located for case (a) at [0, 5, 7], [5, 0, 1] and [10, 6, 8], for case (b) at [0, 1, 7], [1, 0, 1], [5, 0, 8], and for case (c) at [0, 9, 2], [1, 10, 8] [3, 10, 4]. We observe that for (a) there is an area located between the RISs where the PEB takes lower values than the rest of the grid. Comparing case (a) with cases (b) and (c), it is obvious that by locating the RISs towards one corner of the room, the area showing lower PEB, moves to that specific corner. Moreover, by placing the RISs closer to each other in case (c) than in case (b), the low-PEB area becomes more pronounced. We conclude that the location of the RISs plays an important role for the performance of localization and by optimizing their placement one could optimize the localization in certain areas.

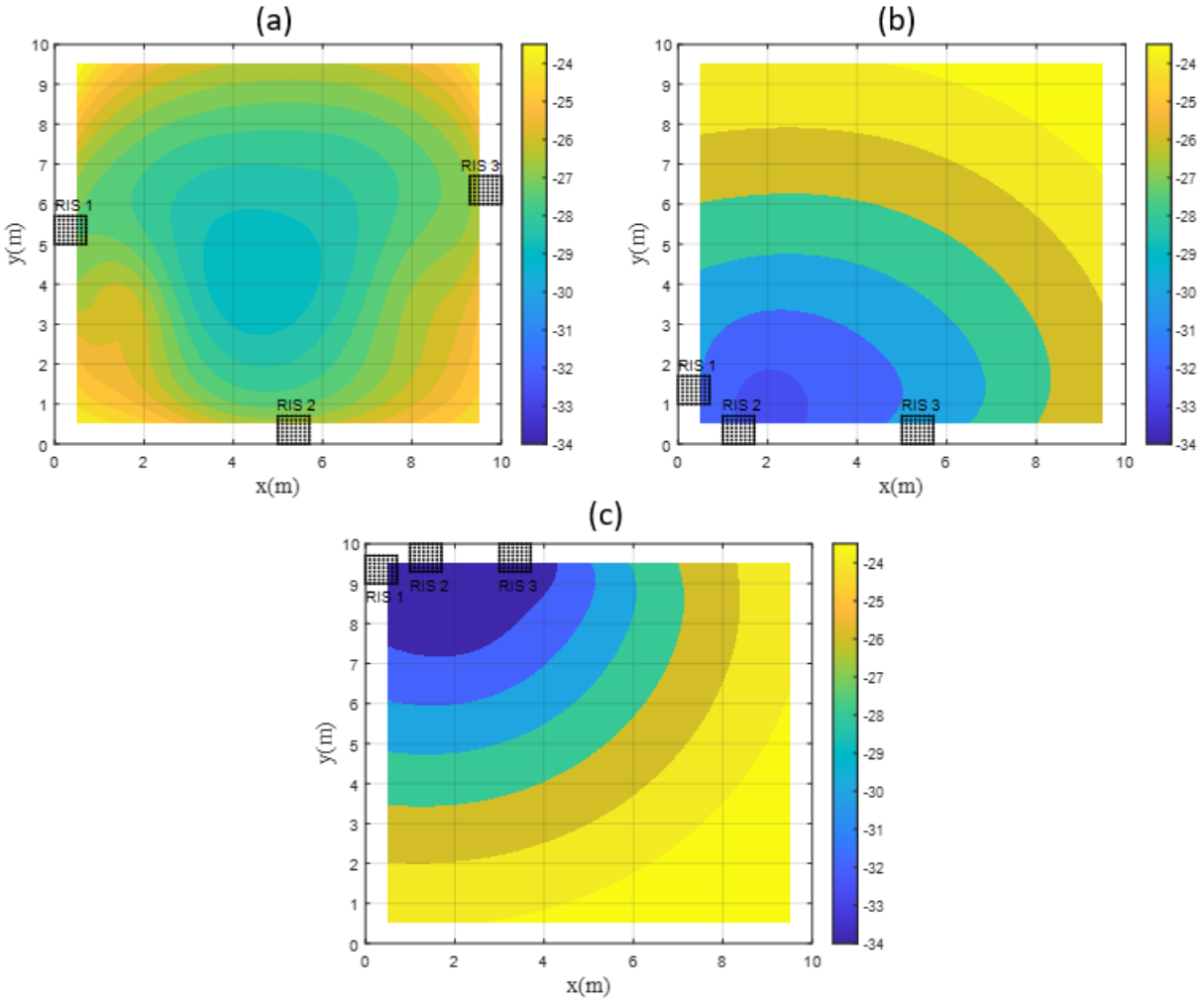

Figure 3-15 – Examples of PEB (in dB) for an Indoor Localization system with 3 RISs in receive mode located for (a) at [0, 5, 7], [5, 0, 1], [10, 6, 8], for (b) at [0,1,7], [1,0,1], [5,0,8], and for (c) at [0, 9, 2], [1, 10, 8] [3, 10, 4].

3.2.6 Localization-Boosted Area of Influence

The **Localization-boosted area of influence** (LB-AoI) is another 2D representation visualizing and quantifying where RIS would improve the *nominal accuracy of a standard system/technology*, which is already operating in favourable conditions (e.g., showing that, given an a priori BS deployment, RIS can timely/locally improve the accuracy to fulfill specific users/application requirements). The LB-AoI can thus be simply defined as the area where the achievable error with RISs is lower than that with no RIS. Just like the LE-AoI, it can be typically represented as a binary contour plot in 2D.

We detail hereafter the example of PEB with multiple BS(s) and multiple RISs in reflection mode. In Figure 3-16 (a)-(d), we show additional examples of PEB contour plots illustrating both RIS-boosted localization performances and RIS-aided low-profile localization in a SISO system through the use of RISs in reflection mode. In these examples, we assume a transmit power of 0.1 mW (-10 dBm) at active BS(s), 3 successive DL transmissions over 1500 subcarriers with a frequency spacing of 240 kHz (thus, with a bandwidth of 360 MHz) per estimate per BS, a RIS size of 128 elements (set as a linear array), free-space propagation in all 2D locations systematically, as well as the possibility to exploit the near-field regime for location estimation.

First, on Figure 3-16 (a), we show the PEB of a reference system (i.e., non-RIS baseline) with 3 BS(s) located in [1, 19], [17, 17], and [8, 1]. On Figure 3-16 (b), we show the PEB while using one additional RIS in [10.0], when the RIS-reflected path is used all over the scene. In this case, we show that the gain is thus mostly noticeable when the UE is close enough from the 3rd transmitting BS, while it is more marginal in the rest of the scene (where direct path contributions are by far dominating). In Figure 3-16 (c), we show the PEB while assuming the presence of a 2nd RIS in [12, 0], while removing one of the 3 BS(s). In this case, we show that, in comparison with the conventional system based on 3 active BS(s), even if the performance is obviously globally degraded over a large portion of the 2D scene, the performance is still maintained at a fairly good level in a significant spatial sub-area close to the 2 RISs (i.e. offering a performance level comparable to that achieved in the inner part of the scene, when using the 3 active BS(s) in Figure 3-16 (a)), thus demonstrating lower-profile localization capabilities (i.e., strictly adapted to local needs). Finally, while using the direct paths from the 3 available BS(s) systematically, but while making deliberately selective/parsimonious usage of an additional RIS-reflected path in a small sub-area (represented as a black rectangular area in the shown example), we illustrate the possibility to create arbitrary localization-boosted sub-areas, which can be particularly relevant for multi-accuracy service provision (e.g., for Industry 4.0 applications).

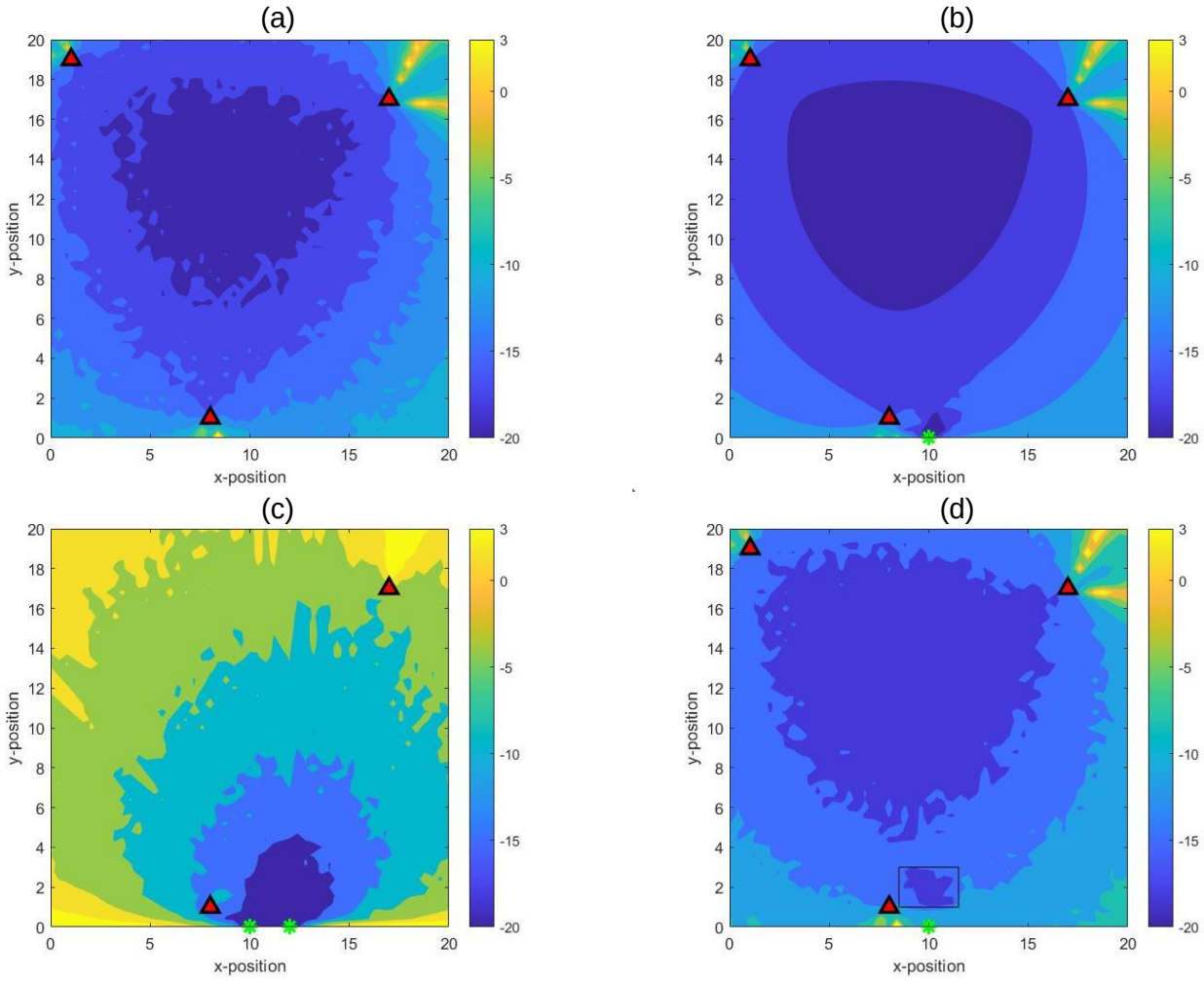

Figure 3-16 – Example of PEB (in dB) for (a) a conventional localization system with 3 BS(s) in [1, 19], [17, 17], and [8, 1], (b) a RIS-boosted localization system with the 3 previous BS(s) and one single RIS in [10, 0], (c) a RIS-aided low-profile localization system with 2 active BS(s) only and a second RIS in [12, 0] and, finally, (d) the creation of an arbitrary localization-boosted sub-

area assuming the selective use of the 1st RIS in addition to BS(s) in the black rectangular area only (and of the 3 BS(s) only over the rest of the scene).

4 Conclusions

According to the objectives of WP2 current document summarizes the first results of the activity devoted to identifying traditional and defining beyond-SoTA relevant performance metrics and target KPIs, to be used by the technical WPs to assess the performance of RISE wireless systems for different scenarios.

A generic DL system model has been described as a basis to provide the definitions for various performance metrics (the corresponding UL system model can be derived in a similar manner) to be used for evaluating the performance benefits brought by RISs: signal to noise (and interference) ratio, latency, communication reliability, channel estimation accuracy, localization accuracy and integrity, energy efficiency, electromagnetic field exposure efficiency, secrecy spectral efficiency.

The concept of “Area of Influence” as the area of significant improvement of wireless connectivity enabled by the RIS technology has been introduced and some analysis have been performed on it. Current simulation results show that the improvement brought by the RIS optimization, with respect to each of the considered connectivity metrics, is localized in space. Furthermore, in a common setup made of a single TX, a single RIS, a single intended RX and potentially an attenuator/blocker, after having optimized the system parameters for the position of the nominal intended RX, the substantial improvement of the performance, which lies on the path of the RIS-RX link (as well as the TX-RIS link, in case there is no attenuator), has been visually demonstrated for all metrics in a Ricean-faded channel with a string LoS component.

5 References

[AKW+21] G. C. Alexandropoulos, K. Katsanos, M. Wen, and D. B. da Costa, "Safeguarding MIMO communications with reconfigurable metasurfaces and artificial noise," in Proc. *IEEE International Conference on Communications*, Montreal, Canada, 14–18 June 2021, pp. 1-6.

[CDP+20] An. Clemente, F. Diaby, Di Palma, L. Dussopt and R. Sauleau“Experimental validation of a 2-bit reconfigurable unit-cell for transmitarrays at Ka-band,” IEEE Access, vol.8, pp.114991-114997, 2020.

[CDS+12] A. Clemente, L. Dussopt, R. Sauleau, P. Potier and P. Pouliguen, "1-Bit Reconfigurable Unit Cell Based on PIN Diodes for Transmit-Array Applications in X -Band," in IEEE Transactions on Antennas and Propagation, vol. 60, no. 5, pp. 2260-2269, May 2012, doi: 10.1109/TAP.2012.2189716.

[CDS+13] A. Clemente, L. Dussopt, R. Sauleau, P. Potier and P. Pouliguen, "Wideband 400-Element Electronically Reconfigurable Transmit array in X Band," in IEEE Transactions on Antennas and Propagation, vol. 61, no. 10, pp. 5017-5027, Oct. 2013, doi: 10.1109/TAP.2013.2271493.

[DCS+20] F. Diaby, A. Clemente, R. Sauleau, K. Pham and L. Dussopt “2-bit reconfigurable unit-cell and electronically steerable transmit arrayat Ka-band,” IEEE Transaction Antennas and Propag., vol.68, no.6, pp.5003-5008, Jun.2020.

[DPC+17] L. Di Palma, A. Clemente, L. Dussopt, R. Sauleau, P. Potier and P.Pouliguen“Circularly-polarized reconfigurable transmit array in Ka-bandwith beam scanning and polarization switching capabilities,” IEEE Transaction on Antennas and Propag., Vol.65, no.2, pp.529-540, Feb.2017.

[HZA+19] C. Huang, A. Zappone, G. C. Alexandropoulos, M. Debbah and C. Yuen, "Reconfigurable Intelligent Surfaces for Energy Efficiency in Wireless Communication," in IEEE Transactions on Wireless Communications, vol. 18, no. 8, pp. 4157-4170, Aug. 2019, doi: 10.1109/TWC.2019.2922609.

[FPH+21] R. Fara, D.-T. Phan Huy, P. Ratajczak, A. Ourir, M. Di Renzo, J. de Rosny “Reconfigurable Intelligent Surface-Assisted Ambient Backscatter Communications - Experimental Assessment,” accepted to IEEE’2021. Available at: https://arxiv.org/ftp/arxiv/papers/2103/2103.08427.pdf

[RBF+10] P. Ratajczak, J. M. Baracco and P. Brachat, "New measurement method of the reflection phase coefficient of High Impedance Surface," Proceedings of the Fourth European Conference on Antennas and Propagation, Barcelona, Spain, 2010, pp. 1-4.

[RBF+13] P. Ratajczak, P. Brachat, J. Fargeas and J. Baracco, "C-band active reflectarray based on high impedance surface," 2013 IEEE International Symposium on Phased Array Systems and Technology, Waltham, MA, USA, 2013, pp. 570-576, doi: 10.1109/ARRAY.2013.6731892.

[ZDR+21-1] Al. Zappone, M. Di Renzo, F. Shams, X. Qian, M. Debbah “Overhead-Aware Design of Reconfigurable Intelligent Surfaces in Smart Radio Environments”. Available at https://arxiv.org/pdf/2003.02538.pdf

[ZDR+21-2] Al. Zappone, M. Di Renzo, F. Shams, X. Xi, M. Debbah “On The Optimal Number of Reflecting Elements for Reconfigurable Intelligent Surfaces” available at https://arxiv.org/pdf/2007.07665.pdf